Biological and Medical Applications of Materials and Interfaces

Metal-Organic Frameworks as Drug Delivery Platforms for Ocular Therapeutics

Jesus Gandara-Loe, Isabel Ortuño-Lizarán, Laura Fernández-Sanchez, Jorge L Alio, Nicolas Cuenca, Alfredo Vega Estrada, and Joaquin Silvestre-Albero

ACS Appl. Mater. Interfaces, **Just Accepted Manuscript** • DOI: 10.1021/acsami.8b20222 • Publication Date (Web): 18 Dec 2018

Metal-Organic Frameworks as Drug Delivery Platforms for Ocular Therapeutics

Jesús Gandara-Loe,[a] Isabel Ortuño-Lizarán,[b] Laura Fernández-Sanchez,[c] Jorge L. Alió,[d] Nicolás Cuenca,[b] Alfredo Vega-Estrada,[d] and Joaquín Silvestre-Albero[a,]*

[a]Laboratorio de Materiales Avanzados, Departamento de Química Inorgánica-IUMA, Universidad de Alicante, E-03690 San Vicente del Raspeig, Spain

[b]Departamento de Fisiología, Genética y Microbiología, Universidad de Alicante, E-03690 San Vicente del Raspeig, Spain

[C]Departamento de Óptica, Farmacología y Anatomía, Universidad de Alicante, E-03690 San Vicente del Raspeig, Spain

[d]Research and Development Department, VISSUM Corporation, E-03016 Alicante, Spain

KEYWORDS: MOFs, Amorphization, Glaucoma treatment, Drug delivery, Ocular therapeutics

ABSTRACT

Metal-organic frameworks (MOFs) have been evaluated as potential nanocarriers for intra-ocular incorporation of brimonidine tartrate to treat chronic glaucoma. Experimental results show that UiO-67 and MIL-100 (Fe) exhibit the highest loading capacity with values up to 50-60 wt.%, while the performance is quite limited for MOFs with narrow cavities (below 0.8 nm, e.g. UiO-66 and HKUST-1). The large loading capacity in UiO-67 is accompanied by an irreversible structural amorphization in aqueous and physiological media that promotes extended release kinetics above 12 days. Compared to the traditional drawbacks associated with the sudden release of the commercial drugs (e.g., ALPHAGAN), these results anticipate UiO-67 as a potential nanocarrier for drug delivery in intra-ocular therapeutics. These promising results are further supported by cytotoxicity tests using retinal photoreceptor cells (661W). Toxicity of these structures (including the metal nodes and organic ligands) for retinal cells is rather low for all samples evaluated, except for HKUST-1.

1. INTRODUCTION

Glaucoma is the second leading cause of irreversible blindness worldwide with millions of people, aged 40 and older, affected by its common form, open-angle glaucoma.[1] After an initial diagnosis, medication is the main treatment nowadays to halt further loss of vision. Glaucoma is a multifactorial disease, usually associated to an increased pressure within the eye, and the associated damage in the optical nerve, resulting in vision impairment and even blindness. Among the different drugs available in the market, brimonidine is one of the most widely applied.[2] Brimonidine is an alpha adrenergic receptor agonist that, upon topical administration, can reduce intraocular pressure (IOP) by reducing aqueous humour production and increasing

uveoscleral outflow. Recent studies have shown that brimonidine has no adverse effects on different retinal cells, but rather it shows neuroprotective effects on retinal ganglion cell degeneration in glaucoma.[3,4] In fact, these and other results together with clinical trials have derived in the commercialization of brimonidine for the treatment of glaucoma under European medication agency (EMA) mandate (REF: EMA/366180/2017). Despite the high benefits of the drug, topical administration is usually associated with important drawbacks such as poor bioavailability (only 5% of the administered drug reaches the interior of the eye), side effects due to rapid drainage through nasolacrimal duct, and the necessity for multiple administration (2-3 eye drops daily for many years). Taking into account the low compliance of patients to strictly follow the treatment and the detrimental effects in case of breach, new therapies are required to improve the quality of life in patients and to decrease their dependence on external medication.

One of the most promising alternatives for a long-term treatment of glaucoma consist in the incorporation of the drug in platforms or vehicles able to concentrate the drug and release it at the target in a controlled way, increasing the bioavailability and avoiding the traditional "burst effects". These delivery systems include hydrogels[5], microspheres[6], nano-vesicles[7], nanoparticles[8], microfilms[9], among others. Unfortunately, these formulations based on macromolecules or polymers suffer from low loading capacity (gravimetric < 1 wt. % and/or volumetric <0.1 wt./vol. %) and fast release of the drug (within minutes/hours).[10-12] These numbers can be improved through the incorporation of denser inorganic matrices in the formulation, for instance montmorillonite clay and layered double hydroxides (LDH).[13,14] Montmorillonite/chitosan nanoparticles have been evaluated as delivery systems for betaxolol hydrochloride, a selective beta-adrenergic blocking agent, with excellent values of drug loading capacity (up to 14.5 wt.%) and delivery kinetics between 6-10h.[13] Sun et al. reported the

synthesis of composites using a thermogel incorporated with brimonidine-loaded LDH nanoparticles with a significant loading capacity (up to 0.125 mg/g), although lower than the original LDH (25.0 mg/g or 2.5%), and an improved release profile (up to 2 days are required to release 75%) compared to the original LDH.[14] These studies mainly focused in pre-corneal administration, thus keeping the concerns about bioavailability in the interior of the eye (low penetration of the drug through the cornea; < 1-7%).

Taking into account the limited volume of the ocular cavity (< 3-4 cm^3) and the limited allowance of fluid (human eye can hold only 7-10 μl of fluid), any intraocular delivery platform for ocular therapeutics needs to fulfil even more stringent requirements compared to pre-corneal devices such as i) extremely large loading capacity (in gravimetric (wt.%) and volumetric (w/v %) basis) to mitigate any interference in the visual field after dosing, ii) slow delivery kinetics (within days or weeks) to allow long-term therapy, iii) high biocompatibility for retinal cells and, last but not least, iv) structural instability once the material has completed the job.

Potential candidates able to fulfil these requirements are metal-organic frameworks (MOFs). The proper combination of metallic nodes or clusters and organic ligands allows to design a wide variety of 1-3D networks characterized by an extremely large surface area and pore volume.[15] Previous studies described in the literature have shown that MOFs are potential candidates for drug delivery with excellent results for a wide variety of drugs such as antitumoral, retroviral, etc.[16,17] Furthermore, *in vitro* and *in vivo* cytotoxicity assays have anticipated a promising performance with low toxicity and inflammatory activity.[16-18] To our knowledge, MOFs have never been tested as potential drug delivery platforms for ocular therapeutics.

Based on these premises, the main goal of the present study is the evaluation of several MOFs in the adsorption and release of brimonidine for glaucoma treatment, the evaluation of their

structural stability in the charging/discharging media and, last but not least, the evaluation of the cytotoxicity of the different components (bulk MOF, linker and metallic precursors) in retinal photoreceptor culture cells (661W).

2. EXPERIMENTAL SECTION

2.1. Synthesis and characterization of MOFs

UiO-66, UiO-67 and MIL-100(Fe) MOFs have been synthetized based in previous works reported in the literature. UiO-66 and UiO-67 were synthetized based in the procedure reported by Katz et al.[19] For UiO-66, 0.5 g of ZrCl4 were dissolved in 20 mL of DMF and 4 mL of concentrated HCl. In a second vessel, 0.492 g of terephthalic acid (BDC) were dissolved in 40 mL of DMF. The two solutions were mixed and maintain under stirring for 30 min. The transparent final solution was transferred to a 200 mL jar, closed tightly and kept at 353 K overnight. The synthesis procedure for UiO-67 was similar to the one described for UiO-66. Briefly, 0.360 g of 4,4'-biphenyldicarboxylic acid (BDPC) were added to a mixture of 20/2 mL of DMF/concentrated HCl and 0.268 g of $ZrCl_4$ were dissolved into 40 mL of DMF. The two solutions were mixed and stirred for 30 min. The white coloured final solution was placed into a 200 mL jar, closed tightly and kept at 353 K overnight. The resulting solid was filtered and washed first with DMF (2x30 mL) and then with ethanol (2x30 mL). Samples were activated under low vacuum ($13 \cdot 10^3$ Pa) until a temperature of 363 K was reached. The samples were then subjected to an outgassing treatment at 423 K for 3 h under ultra-high vacuum conditions. MIL-100 (Fe) was prepared using the facile low temperature synthesis procedure reported in the literature by Zhang et al.[20] Briefly, 4.04 g of $Fe(NO_3)_3 \cdot 9H_2O$ and 1.89 g of trimesic acid (H_3BTC) were dissolved in 6 mL of distillate water and kept under reflux at 368 K overnight.

The solid was purified three times using a solvent extraction treatment with deionized water (350 ml) and ethanol (350 ml) at 343 K for 24 h, and finally dried in vacuum at 423 K for 10 h. HKUST-1 (Cu) has been used as received from the Sigma-Aldrich, labelled and commercialize as Basolite C 300.

X-ray diffraction patterns of the samples were recorded using a Bruker D8-Advance equipment with mirror Goebel with high temperature Chamber and a generator of X-ray KRISTALLOFLEX K 760-80F with a tube of RX with copper anode. Spectra were registered between 3 and 80° (2θ) with a step of 0.05° and a time per step of 3 s.

Textural properties of the samples were evaluated by gas physisorption of nitrogen at 77 K. Gas adsorption measurements were performed in a homemade fully automated manometric equipment designed and constructed by the Advanced Materials Group (LMA), now commercialized as N2GSorb-6 (Gas to Materials Technologies; www.g2mtech.com). The samples were previously degassed for 8 h at 423 K under vacuum (10^{-3} Pa). Nitrogen adsorption data were used to determine: (i) the total pore volume (V_t) at a relative pressure of 0.95, (ii) the BET specific surface area (S_{BET}) and (iii) the micropore volume (V_{N2}) by application of Dubinin-Radushkevich equation. The difference between V_t and V_{N2} is considered to be the mesopore volume (V_{meso}).

The size and shape of the synthesized crystals was evaluated using field emission scanning electron microcopy (FESEM). These analyses were performed in a Merlin VP Compact system from ZEISS with a resolution of 0.8 nm at 15 kV and 1.6 nm at 1 kV. FTIR spectra were recorded on a JASCO FTIR 4700 spectrometer with a resolution of 2 cm^{-1}.

Structural stability of the MOFs was evaluated by immersing 0.1 g of each MOF in 50 mL of an aqueous solution or a phosphate-based solution (PBS) for 1h, 1 day, 7 days and 30 days. After

this time intervals, the material was washed with ultrapure water and filtered in vacuum. After an evacuation at 393 K for 8 h, the crystallinity of the materials was checked using XRD analysis.

2.2. Loading and release experiments

Brimonidine tartrate quantification was done based on the spectrometric method developed by Bhagav et al.[21] A 1500 ppm stock solution of brimonidine tartrate was prepared dissolving 1.5 g of brimonidine tartrate in 1000 mL of ultrapure water. The calibration curve was constructed measuring concentrations from 2 to 15 ppm using a UV-Vis spectrophotometer (double-beam spectrophotometer with a photomultiplier tube detector JASCO V-650 UV-VIS) at wavelengths of λ_1= 247 nm and λ_2= 320 nm. High performance liquid chromatography (HPLC) was used to certify the precision of the UV-Vis method in brimonidine quantification.[22] Both methods gave an accuracy above 97%, thus confirming the validity of the UV-vis technique for brimonidine determination.

2.2.1. Brimonidine loading experiments

For the loading tests, a group of aqueous solutions with an initial concentration of 200 ppm, 500 ppm, 750 ppm, 1000 ppm and 1500 ppm of brimonidine tartrate were prepared from the stock solution. The MOFs samples were outgassed at 423 K overnight prior to the adsorption measurement. 100 mg of each MOF were placed in contact with 50 mL of each concentration and left under stirring until equilibrium was reached. Aliquots were taken in different periods of time in order to evaluate the kinetic behaviour of each MOF. All samples reached complete equilibrium after 7 h.

The quantification of brimonidine tartrate was determined by UV-Vis spectrophotometry diluting each aliquot 1:100 and using the method described above. A MOF-loaded blank experiment was measured to determine possible interferences in the UV-vis signal due to the MOF degradation. However, no interferences were observed at the wavelengths selected for brimonidine for all MOFs evaluated.

2.2.2. Brimonidine release experiments

In an initial step the MOFs were loaded by contacting 100 mg of a degassed MOF with 50 mL of a 500 ppm brimonidine tartrate aqueous solution. The system was left under stirring for 7 h to ensure full equilibrium. After this time, the sample was collected by filtration and an aliquot was saved to determine the maximum loading amount. The brimonidine-loaded MOF was washed several times with ultrapure water and dried under vacuum at 333 K for 6 h. The dried brimonidine-loaded MOF was immersed in 50 mL of physiological solution (PBS) and aliquots were taken at different times up to 12 days. Brimonidine determination has been performed in a similar procedure to that described above. All the dilutions (1:100) and calibration curve were measured using PBS as a solvent instead of ultrapure water.

2.3. Cytotoxicity tests

661W cell line, derived from mouse retinoblastoma and considered a photoreceptor cell line, was employed in the cytotoxicity tests. To assess MOFs toxicity in retinal cells, 611W cells were incubated with MOFs and MOFs components at different concentrations for 24h or 48h. A death control was also included in each study to be sure that cells die with a noxious stimulus (0.4 mM sodium nitroprusside, SNP; 228710, Sigma-Aldrich, St Louis, MO, USA).

First, for cell viability assays at 24h or 48h after adding the MOFs, cells were plated in 96-well plates at a density of 10000 or 4000 cells per well respectively. They were incubated in Dulbecco's modified Eagle's medium (DMEM High Glucose; L0106, Biowest, Nuaillé, France) supplemented with 10% fetal bovine serum (FBS; SV30160, GE Healthcare, Pasching, Austria), 1% penicillin/streptomycin (P9781, Sigma-Aldrich) and 1% L-Glutamine (25030-081, Gibco, Paisley, UK), and maintained during the whole experiment at 310 K in a humidified atmosphere with 5% CO_2. 24 h after seeding, medium was replaced and 0.4 mM SNP or MOF concentrations of 0, 10, 20, 30, 40 and 50 μg/ml in supplemented DMEM were added. Each condition was done at eight replicates per plate. MOFs and their respective components were maintained in the medium and cell viability was assessed at 24 and 48 hours using the XTT cell viability assay (X4626, Sigma-Aldrich). Briefly, this kit consists of a colorimetric assay dependent of a redox reaction that measures mitochondrial activity and thus is an estimate of cell quantity. 100 μl of XTT was added to each well, incubated at 310 K and 5% CO_2 for 2 hours and absorbance measured at 492 nm in a Beckman Coulter AD340 plate reader (Beckman Coulter Inc., Nyon, Switzerland). Absorbance was transformed into viability percentage considering the value of the 0 μg/ml concentration (positive control) as 100% cell viability. All these procedures were done in sterile conditions, using sterile materials and solutions, and MOFs were heat-sterilized at 423 K for 3 hours prior to use.

3. RESULTS AND DISCUSSION

Four different MOFs have been selected for this study, i.e. HKUST-1, MIL-100 (Fe), UiO-66 and UiO-67. The main goal is to evaluate systems with a different porous structure (from purely microporous to micro/mesoporous systems) and different surface chemistry to evaluate the role

of these parameters in the loading and delivery performance. Furthermore, these MOFs have been selected based in the *a priori* low toxicity of the metal species incorporated: zirconium chloride lethal dose LD_{50} ~3500 mg/kg (for UiO-66 and UiO-67), and iron nitrate lethal dose LD_{50} ~3250 mg/kg (for MIL-100(Fe)), except HKUST-1 with a potential toxicity due to the cupper nitrate used (LD_{50} ~940 mg/kg).[23] The selection of HKUST-1 is based on the excellent performance that has been reported in the literature for this material for a wide range of applications, e.g. methane and hydrogen storage,[24-26] hydrocarbon separation,[27] etc. Briefly, HKUST-1 is assembled from $Cu_2(H_2O)_2$ dimer units and tridentate trimesate groups to form 3D channels with alternating cavities of diameter ~1.4 nm and ~1.1 nm connected through pore windows of ~1.0 nm.[28] There are also smaller diameter cavities of ~0.5 nm between the larger cavities. MIL-100 (Fe) consist on trimers of metal octahedra and trimesic acid as a linker.[16] This material possesses cages in the mesoporous range (diameter ~2.5 and ~2.9 nm), accessible through pore windows of 0.48 x 0.58 nm, for the small cage, and 0.86 nm, for the larger one. Finally, UiO-66 and UiO-67 are constituted by clusters of $Zr_6O_4(OH)_4(CO_2)_{12}$ connected through benzene-dicarboxylate and biphenyl-dicarboxilate linkers, respectively. The longer linker in the last case gives rise to larger tetrahedral and octahedral microporous cages, i.e. 0.75 nm and 1.2 nm, for UiO-66, and 1.2 nm and 1.6 nm, for UiO-67. Figure S1 shows a schematic drawing of the evaluated MOFs.

Table 1. Textural properties of the synthesized MOFs.

Sample	S_{BET} (m^2/g)	V_0 (cm^3/g)	V_t (cm^3/g)
HKUST-1	1690	0.65	0.72
MIL-100 (Fe)	1360	0.42	0.79
UiO-66	1465	0.53	0.69
UiO-67	2620	1.02	1.24

The textural characteristics of the synthesized materials have been evaluated using nitrogen adsorption at cryogenic temperatures. These measurements are mandatory to certify the validity of the synthesis method applied and to confirm the quality of the synthesized nanocrystals. Figure S2 shows the N_2 adsorption/desorption isotherms at 77 K for the four samples evaluated. The nitrogen adsorption capacity for samples HKUST-1, MIL-100 (Fe) and UiO-66 is rather similar, i.e. around 350-400 cm^3/g, although with some differences in the shape of the isotherm (knee at low relative pressures). While it is narrower for HKUST-1 and UiO-66 as corresponds to purely microporous materials, the knee is wider and associated with a significant slope in the mid-pressure region in the specific case of the micro/mesoporous MIL-100 (Fe). Compared to UiO-66, longer linkers in UiO-67 give rise to a two-fold increase in the adsorption capacity up to 800 cm^3/g. The presence of larger cages (~1.6 nm) in the case of UiO-67 can be clearly appreciated by a sudden jump in the nitrogen adsorption isotherm at $p/p_0 \sim 0.2$ (right after the filling of the narrow cages). The textural characteristics obtained after application of the BET and the Dubinin-Radushkevich (DR) equations are collected in Table 1. The reported values are in close agreement with the literature, thus validating the synthesis procedure.

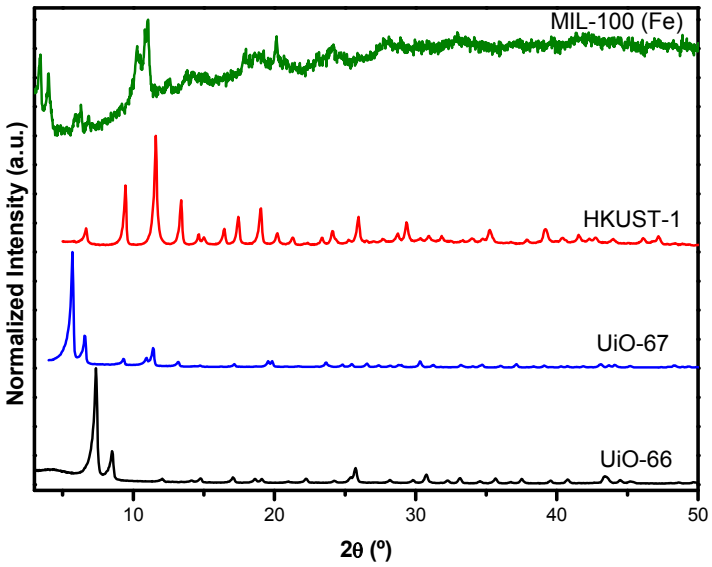

Figure 1. X-ray diffraction pattern of the different MOFs evaluated.

In addition to the textural properties, the crystallinity of the synthesized MOFs has been evaluated using X-ray diffraction. Figure 1 shows the XRD pattern for each of the four MOFs evaluated in the 2Θ range 2-50º. These patterns perfectly match those described in the literature for these materials, thus confirming the quality of the synthesized metal-organic frameworks.

The size and shape of the synthesized nanocrystals have been evaluated using FESEM. The morphology of the synthesized nanocarriers, preferentially the crystal size, is of paramount importance in ophthalmological applications to minimize potential disruption in the visual field upon injection and/or undesired sedimentation in the ocular cavity. Figure S3 shows representative images for the MOFs evaluated. As it can be observed, MIL-100 (Fe), UiO-66 and UiO-67 are constituted by nanometer size crystals (average crystal size 140 ± 30 nm, 80 ± 10 nm and 120 ± 20 nm, respectively). Only HKUST-1 exhibits larger crystals in the micrometer size range (average crystal size 3 ± 1 μm).

Last but not least, the vibrational modes of the synthesized MOFs have been evaluated using FTIR (Figure S4). FTIR spectra constitute a fingerprint to further certify the quality of the synthesized MOFs, including the surface functional characteristics. The four samples evaluated exhibit similar vibrational bands in the 1300-1700 cm^1 range attributed to the structural carboxylate groups in the linkers.[29] More specifically, the peaks around 1368 cm^{-1} and 1448 cm^{-1} corresponds to symmetric stretching vibrations of the carboxylate group (O-C-O groups), whereas the asymmetric vibrations in the carboxylate appears close to 1550-1650 cm^{-1}.[30] Vibration peaks corresponding to the aromatic ring (C=C) are shown at ca. 1500 cm^{-1}, whereas bands attributed to the metal cluster and the linkers appear at lower wavenumbers (1000-500 cm^{-1}).[31] UiO-66 and UiO-67 exhibit longitudinal and transverse modes of Zr-O vibrations between 660 and 540 cm^{-1} and the OH and CH bending modes at 770-740 cm^{-1}. MIL-100(Fe) exhibits sharp peaks at 760 cm^{-1} and 709 cm^{-1} due to the linker bending modes and Fe-O cluster vibrations, while HKUST-1 shows a band at 727 cm^{-1} attributed to the Cu-O mode.[32,30] Last but not least, the absence of significant peaks at 1710-1720 cm^{-1} attributed to the C=O stretching vibration of residual trimesic acid suggest the proper purification of the synthesized MOFs.

Once the crystallographic structure and morphology of the different MOFs has been validated and the textural properties confirmed, these materials have been evaluated in the adsorption of brimonidine tartrate. Liquid phase adsorption isotherms have been quantified at 298 K and at ranging concentrations using ultra-pure water as charging media. As it can be appreciated in Figure 2 the amount of drug loaded increases with the concentration of brimonidine in the aqueous solution, except for HKUST-1 and UiO-66 materials where saturation is already reached at concentrations above 800 mg/L. Apparently, MOFs with narrow micropores become quickly saturated, the final loading capacity being around 0.16 g/g. The scenario changes completely for

MOFs with larger micropores/small mesopores such as UiO67 and MIL-100 (Fe). In this specific case, the loading capacity increases with concentration with a loading capacity at 1400 mg/L as high as 0.31 g/g (31 wt.%), for MIL-100 (Fe), and 0.44 g/g (44 wt.%), for UiO-67. Previous studies described in literature for ibuprofen adsorption in MIL-100 (Cr) reported adsorption values around 0.35 g/g, in close agreement with our data.[16] Extrapolation of the adsorption data reported in Figure 2 using the Langmuir equation (dotted line) gives loading values at saturation as high as 0.49 g/g, for MIL-100 (Fe), and 0.63 g/g, for UiO-67. To our knowledge, these are among the best values described in the literature for the adsorption of drugs using metal-organic frameworks.

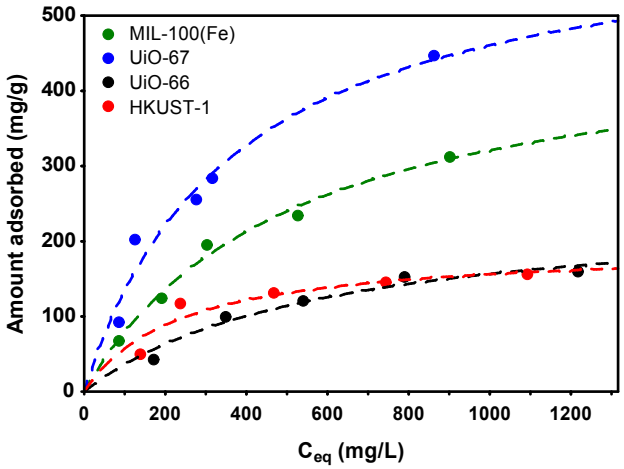

Figure 2. Liquid-phase adsorption isotherms for brimonidine tartrate at 298 K. Fitting to Langmuir equation is included (dotted line).

Adsorption results clearly show that UiO-67, with the larger BET surface area and pore volume (above 1 cc/g), is the best performing material over the whole concentration range

evaluated with a loading capacity superior to the majority of MOFs reported in the literature so far for similar drugs. Despite the significant surface area in HKUST-1, this material becomes saturated immediately with a poor performance at high concentrations. Last but not least, although MIL-100 (Fe) and UiO-66 exhibit similar textural properties (in terms of BET surface area and micropore volume), the presence of mesopores in the former MOF play a crucial role with a loading capacity more than double that of UiO-66. Consequently, these results clearly anticipate that microporous MOFs with a pore size below 0.8 nm are not appropriate for brimonidine adsorption due to the limited accessibility of the drug to the interior cavities. This can also be the reason for the lower loading in MIL-100 (Fe) compared to UiO-67 due to the limited accessibility of the small cages in the former (pore windows of 0.48 x 0.58 nm). In addition to the loading capacity, adsorption kinetics are also relevant. As it can be observed in Figure S5, for an initial concentration of 500 ppm, saturation is reached within 4-5 h, except for UiO-66 with narrow but accessible cavities with adsorption kinetics slightly above 5h. These results are very promising since only a few hours are required to load the materials before injection into the eye.

One of the most relevant issues in medical therapies, not frequently addressed in the literature, concerns the stability of the host structures in the loading and discharging media, i.e. in aqueous solutions or physiological media (PBS). It is well-known in the literature that several MOFs exhibit structural deterioration upon exposure to a humid environment.[33, 34] The instability has been traditionally attributed to the nuclearity, coordination number of the metal, functionality of linker and framework dimensionality. In our case, we have evaluated the structural stability of the different MOFs at different time intervals from 1 day until 30 days using an aqueous solution as a charging media (see Figure S6). At this point it is important to highlight that similar results

have been observed in the presence of a physiological solution of PBS as discharging media. As it can be appreciated, the structural stability highly depends on the nature of the metal-organic network. While HKUST-1 and UiO-67 exhibit a rapid deterioration in the first 24 hours, samples UiO-66 and MIL-100 (Fe) remain stable even after 30 days. The irreversible instability of HKUST-1 is in close agreement with previous findings in the literature in liquid and gas phase.[35, 36] HKUST-1 suffers degradation due to the strong interaction between the open Cu(II) sites (the coordinatively unsaturated sites from the copper paddlewheel) and water molecules. This irreversible instability can explain the low loading capacity for HKUST-1 (see Figure 2), despite the presence of a significant BET surface area in the as-synthesized material. However, the presence of limited accessibility for brimonidine to the inner micropores must also be considered to explain the adsorption results. Contrary to HKUST-1, the results for UiO-67 are more surprising since this material exhibits the best adsorption performance, despite the drastic instability observed in the first few hours. To confirm the potential role of brimonidine within the structure as a stabilizer, we have performed XRD analysis of the loaded material under aqueous solution right after complete saturation, i.e. after 24h. Figure S7 compares the original XRD pattern and the ones after 24h in the presence and absence of the drug. As expected, although the XRD pattern of the loaded MOF already anticipates an important crystallographic deterioration (amorphization), this damage is lower than the one observed in the absence of the drug, i.e. the presence of the brimonidine within the structure seems to be crucial to preserve a certain crystallinity in UiO-67, thus explaining the excellent adsorption results achieved. Upon loading, the second open question concerns the delivery kinetics. Previous studies described in the literature for MOFs have shown that 3-5 days release is a common number for this kind of drugs.[16-18] The main question at this point is the role that instability can exhibit in the release

kinetics. Release kinetics were not evaluated for HKUST-1 due to the strong structural deterioration even in the presence of the drug. Figure 3 shows the amount of brimonidine released in PBS (discharging media) versus time for the loaded UiO-66, UiO-67 and MIL-100 (Fe) materials (loading performed using a 500 ppm brimonidine aqueous solution). As it can be observed, all materials exhibit two regimes related to the location of the drug in the structure. An initial release for 3 days associated with brimonidine weakly bonded within the MOF structure (ca. 70-80% delivery for MIL-100 (Fe) and UiO-66) and a subsequent slow release of brimonidine, although quite limited up to 75-85% during next 6-8 days. The absence of complete release in these two MOFs clearly denotes the presence of brimonidine strongly interacting with the structural framework. Interestingly, the scenario changes completely in the specific case of UiO-67. The structural instability in aqueous and PBS media gives rise to an initial release within 4 days of around 43% and a subsequent and progressive release with time up to a 56% after 12 days. An extrapolation of these values suggest potentially more than 30 days of continuous release with the associated benefits for a chronic ocular disorder such as glaucoma. The beneficial role of the partial amorphization of MOFs in the release kinetics was recently described by Orellana-Tavra et al. for calcein released in mechanically deteriorated UiO-66.[37] More than 30 days controlled release could be obtained versus 2 days in the crystalline counterpart.

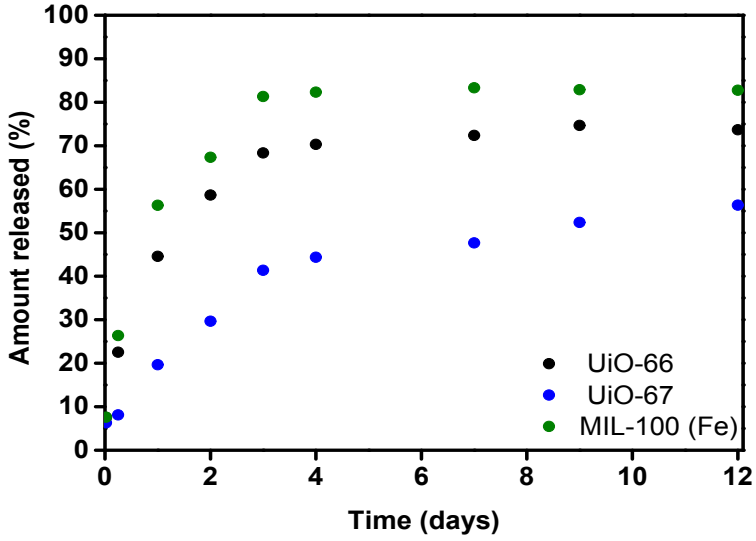

Figure 3. Brimonidine tartrate release kinetics at 298 K in physiological media PBS (loading concentration 500 ppm).

As described in the introduction, the final goal of this study is the design of metal-organic frameworks with a high potential to be applied in glaucoma treatment after injection in the intra-ocular cavity. From this perspective, the progressive deterioration of the MOF within the eye while releasing the drug can be anticipated as an optimum performance to promote the complete clearance of the ocular cavity (absence of disruptions in the visual field) upon completion of the job. To this end, there is a major issue that must be fulfilled, i.e. the MOFs and their respective components (metal nodes and organic linkers) must exhibit a low toxicity towards ocular tissues.

In vitro models based in cell cultures, instead of *in vivo* models, are the first choice to test toxicity of new compounds or nanoparticles, because of their low cost, time efficiency, their trustworthy results, and because they involve no ethical issues.[38]

The 661W cell line (kindly provided by Dr. Muayyad Al-Ubaidi; University of Oklahoma) is derived from retinoblastoma, a mouse retinal tumour.[39] This cell line expresses several markers of photoreceptor cells,[40] that made them one of the most widely used cell line to screen safety and efficacy in a great number of drugs for ocular treatments.[41-44] In fact, Januschowski et. al. suggest that cell lines derived from retinal cells such 661W or ARPE19 cells are the most accurate to evaluate retinal toxicity.[45] Thus, cytotoxicity of MOFs and their components was assessed in 661W cells (Figure 4). As it can be appreciated in Figure 4, except in the specific case of HKUST-1, the cell viability evaluated after 48h exposure is, in all cases, very close to 100 %. These results anticipate that MIL-100 (Fe), UiO-66 and UiO-67 materials do not affect retinal photoreceptor cells viability. Only sample HKUST-1 is toxic for retinal photoreceptor cells (cell viability below 50 %), most probably due to the presence of copper and the important structural deterioration associated.

To confirm this point, the cytotoxicity assays have been extended to the different components of the MOF, i.e. metallic precursors and organic linkers (see Figures S8-S11). These experiments confirm that, with the exception of HKUST-1, cell viability is not affected by any of the MOF components. In addition, the effect of MIL-100 (Fe), UiO-66 and UiO-67 on cells is rather similar with different time incubations, i.e. the viability is maintained at 24h and 48h. This observation suggests that a prolonged interaction between MOFs and cells after intra-ocular injection will not be harmful for cell viability or proliferation. On the contrary, HKUST-1 present time-dependent effects, as a prolonged contact with cells drops cell viability at 48h, when compared to 24h (Figures S8). An evaluation of the HKUST-1 components clearly show that the metal precursor (copper nitrate) is the one responsible for the high toxicity of the MOF.

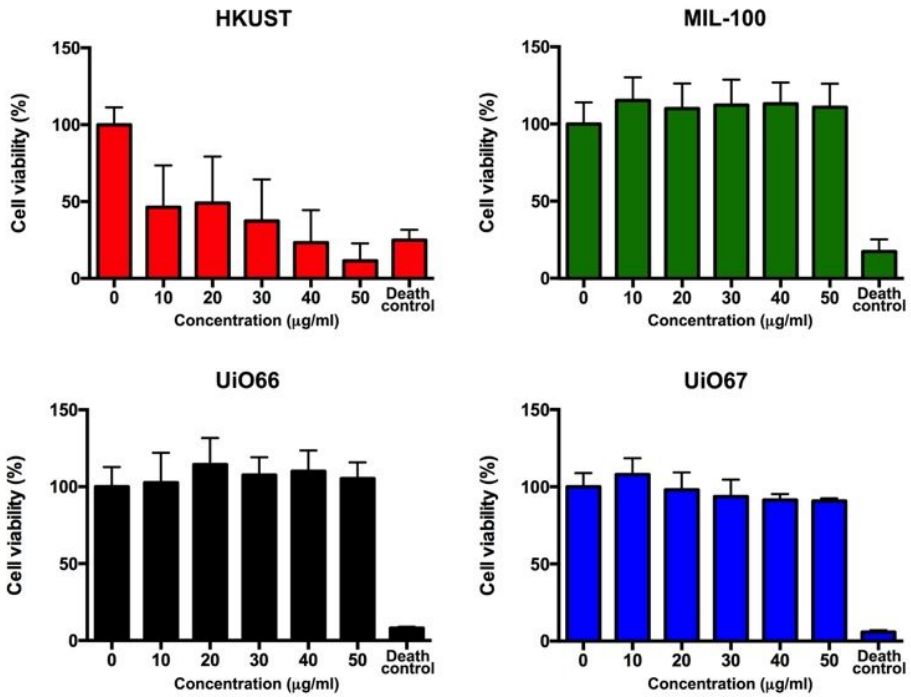

Figure 4. Cytotoxicity tests for the different MOFs evaluated using a retinal photoreceptor cell line (661 W) at 48h.

In summary, metal-organic frameworks can be anticipated as potential nanocarriers for drug delivery in ocular therapeutics. The proper selection of the metallic node and the organic linker allows to improve the loading capacity to values above 50 wt.%, in the specific case of UiO-67 and MIL-100 (Fe). Furthermore, the associated amorphization observed for UiO-67 in aqueous media becomes an advantage to extend the delivery kinetics up to 12 days or above. Taking into account that a patient with glaucoma requires 2-3 drops of brimonidine per day (2 mg/mL solution- ALPHAGAN), this corresponds to 0.3 mg per day or 4.5 mg every 15 days. Assuming a loading capacity for UiO-67 of 630 mg/g, patients will require the injection of 7 mg of loaded MOF every 15 days, i.e. 10 μl of MOF (considering the crystallographic density of 0.708 g/cm^3).

Interestingly, these numbers are *a priori* within the theoretical threshold that human eye can hold. However, as the bioavailability of the drops is quite low (< 10%), these numbers could be even reduced for an intra-ocular administration (considering 100% bioavailability) up to 1 order of magnitude, thus validating the potential of the proposed approach.

Furthermore, in vitro cytotoxicity results confirm the validity of our approach for drug delivery in intraocular treatments without inducing damage in photoreceptor retinal cells. These results are encouraging in terms of drug dosage and long-term delivery. However further experiments in vivo would be useful to assess the possible reaction of retinal tissue to MOFs, such as microglial activation or gliosis, due to an eventual accumulation of MOF metal nodes during long-term treatments.

CONCLUSIONS

Metal-organic frameworks (MOFs) can be anticipated as promising nanodevices for drug delivery in ocular therapeutics. Experimental results have shown that samples combining wide micropores and/or small mesopores are able to achieve a high loading capacity, above 50 wt.% (MIL-100(Fe) and UiO-67), for an alpha adrenergic receptor agonist such as brimonidine. Furthermore, delivery kinetics have shown that the associated amorphization in the case of UiO-67 upon ultrapure water or PBS exposure, as suggested by XRD measurements, can be very helpful to extends the delivery kinetic up to 12 days or above. Last but not least, cytotoxicity assays using retinal photoreceptor cells show a high biocompatibility for the MOFs evaluated, except HKUST-1, thus paving the way towards the application of MOFs in intra-ocular therapeutics.

ASSOCIATED CONTENT

Physico-chemical characterization of the MOFs (nitrogen adsorption isotherms, F-SEM, FTIR analysis), structural stability of MOFs in aqueous solution, brimonidine tartrate loading kinetics and cytotoxicity evaluation of MOFs, linkers and metal precursors are included in the Supporting Information.

AUTHOR INFORMATION

Corresponding Author

*Joaquin Silvestre-Albero; Email: joaquin.silvestre@ua.es

ORCID

Jesús Gandara Loe: 0000-0003-1334-4788

Isabel Ortuño Lizarán: 0000-0003-1083-9259

Laura Fernández Sánchez: 0000-0002-3629-0156

Nicolas Cuenca: 0000-0002-6767-5710

Joaquín Silvestre Albero: 0000-0002-0303-0817

Notes

The authors declare no competing financial interest.

Author Contributions

JGL and JSA did the preparation and characterization of the different MOFs evaluated, including the drug loading and release experiments. IOL and LFS were responsible for the cytotoxicity tests for the MOFs and the individual components. These tests were coordinated and discussed

by NC. AVE and JLA supplied the drug and participated together with JSA in the coordination and discussion of this study.

ACKNOWLEDGMENT

Authors would like to acknowledge financial support from MINECO (MAT2016-80285-p), GV (PROMETEOII/2014/004), H2020 (MSCA-RISE-2016/NanoMed Project). JGL acknowledges GV (GRISOLIAP/2016/089) for the research contract. NC acknowledges financial support from MINECO (MINECO-FEDER-BFU2015-67139-R) and GV (Prometeo 2016/158). IOL acknowledges Ministerio de Educación, Spain (FPU 14/03166).

REFERENCES

(1) Glaucoma Research Foundation, https://www.glaucoma.org, accessed on September 2018.

(2) Greenfield, D.S.; Liebmann, J.M.; Ritch, R. Brimonidine: A New Alpha2-Adrenoreceptor Agonist for Glaucoma Treatment. *J. Glaucoma* **1997**, *6*, 250-258.

(3) Beltramo, E.; Lopatina, T.; Mazzeo, A.; Arroba, A.I.; Valverde, A.M.; Hernández, C.; Simó, R.; Porta, M. Effects of the Neuroprotective Drugs Somatostatin and Brimonidine on Retinal Cell Models of Diabetic Retinopathy. *Acta Diabetol* 2016, *53*, 957-964.

(4) Lambert, W.S.; Ruiz, L.; Crish, S.D.; Wheeler, L.A.; Calkins, D.J. Brimonidine Prevents Axonal and Somatic Degeneration of Retinal Ganglion Cell Neurons. *Mol. Neurodegener* 2011, *6*, 4.

(5) Cho, I.S.; Park, C.G.; Huh, B.K.; Cho, M.O.; Khatun, Z.; Li, Z.; Kang, S.-W.; Choy, Y.B.; Huh, K.M. Thermosensitive Hexanoyl Glycol Chitosan-based Ocular Delivery System for Glaucoma Therapy. *Acta Biomater.* **2016**, *39*, 124-132.

(6) Chiang, B.; Kim, Y.C.; Doty, A.C.; Grossniklaus, H.E.; Schwendeman, S.P.; Prausnitz, M.R. Sustained Reduction of Intraocular Pressure by Supraciliary Delivery of Brimonidine-Loaded Poly(lactic acid) Microspheres for the Treatment of Glaucoma. *J. Controlled Release* **2016**, *228*, 48-57.

(7) Prabhu, P.; Nitish, K.R.; Koland, M.; Harish, N.M.; Vijayanarayan, K.; Dhondge, G.; Charyulu, R.N. Preparation and Evaluation of Nano-vesicles of Brimonidine Tartrate as an Ocular Drug Delivery System. *J. Young. Pharm.* **2010**, *2*, 356-361.

(8) Ibrahim, M.M.; Abd-Elgawad, A.-E.; Soliman, O.A.; Jablonski, M.M. Novel Topical Ophthalmic Formulations for Management of Glaucoma. *Pharm. Res.* **2013**, *30*, 2818-2831.

(9) Manickavasagam, D.; Wehrung, D.; Chamsaz, E.A.; Sanders, M.; Bouhenni, R.; Crish, S.D.; Joy, A.; Oyewumi, M.O. Assessment of Alkoxylophenacyl-based Polycarbonates as a Potential Platform for Controlled Delivery of a Model Anti-glaucoma. *Europ. J. Pharma. Biopharma.* **2016**, *107*, 56-66.

(10) Wadhma, S.; Paliwal, R.; Paliwal, S.R.; Vyas, S.P. Nanocarriers in Ocular Drug Delivery: An Update Review. *Curr. Pharm. Des.* **2009**, *15*, 2724-2750.

(11) Jiang, S.; Franco, Y.L.; Zhou, Y.; Chen, J. Nanotechnology in Retinal Drug Delivery. *Int. J. Ophthalmol.* **2018**, *11*, 1038-1044.

(12) Bachu, R.D.; Chowdhury, P.; Al-Saedi, Z.H.F.; Karla, P.K.; Boddu, S.H.S. Ocular Drug Delivery Barriers - Role of Nanocarriers in the Treatment of Anterior Segment Ocular Diseases. *Pharmaceutics* **2018**, *10*, 28.

(13) Li, J.; Tian, S.; Tao, Q.; Zhao, Y.; Gui, R.; Yang, F.; Zang, L.; Chen, Y.; Ping, Q.; Hou, D. Montmorillonite/Chitosan Nanoparticles as a Novel Controlled-release Topical Ophthalmic Delivery System for the Treatment of Glaucoma. *Int. J. Nanomedicine* **2018**, *13*, 3975-3987.

(14) Sun, J.; Lei, Y.; Dai, Z.; Liu, X.; Huang, T.; Wu, J.; Xu, Z.P.; Sun, X. Sustained Release of Brimonidine from a New Composite Drug Delivery System for Treatment of Glaucoma. *ACS Appl. Mater. Interfaces* **2017**, *9*, 7990-7999.

(15) Zhou, H.-C.; Long, J.R.; Yaghi, O.M. Introduction to Metal-Organic Frameworks. *Chem. Rev.* **2012**, *112*, 673-674.

(16) Horcajada, P.; Serre, C.; Vallet-Regí, M.; Sebban, M.; Taulelle, F.; Férey, G. Metal-Organic Frameworks as Efficient Materials for Drug Delivery. *Angew. Chem. Int. Ed.* **2006**, *45*, 5974-5978.

(17) Horcajada, P.; Chalati, T.; Serre, C.; Gillet, B.; Sebrie, C.; Baati, T.; Eubank, J.F.; Heurtaux, D.; Clayette, P.; Kreuz, C.; Chang, J.-S.; Hwang, Y.K.; Marsaud, V.; Bories, P.-N.; Cynober, L.; Gil, S.; Ferey, G.; Couvreur, P.; Gref, R. Porous Metal-Organic-Framework Nanoscale Carriers as a Potential Platform for Drug Delivery and Imaging. *Nature Mater.* **2010**, *9*, 172-178.

(18) Abuçafy, M.P.; Caetano, B.L.; Chiari-Andréo, B.G.; Fonseca-Santos, B.; do Santos, A.M.; Chorilli, M.; Chiavacci, L.A. Supramolecular Cyclodextrin-based Metal-Organic Frameworks as

Efficient Carrier for Anti-inflammatory Drugs. *Europ. J. Pharma. Biopharma.* **2018**, *127*, 112-119.

(19) Katz, M.J.; Brown, Z.J.; Colón, Y.J.; Siu, P.W.; Scheidt, K.A.; Snurr, R.Q.; Hupp, J.T.; Farha, O.K. A Facile Synthesis of UiO-66, UiO-67 and Their Derivatives. *Chem. Commun.* **2013**, *49*, 9449-9451.

(20) Zhang, F.; Shi, J.; Jin, Y.; Fu, Y.; Zhong, Y.; Zhu, W. Facile Synthesis of MIL-100(Fe) Under HF-free Conditions and its Application in the Acetalization of Aldehydes with Diols. *Chem. Eng. J.* **2015**, *259*, 183-190.

(21) Bhagav, P.; Deshpande, P.; Pandey, S.; Chandran, S. Development and Validation of Stability Indicating UV Spectrophotometric Method for the Estimation of Brimonidine Tartrate in Pure Form, Formulations and Preformulation Studies. *Der Pharm. Lett.* **2010**, *2*, 106-122.

(22) Popaniya, H.S.; Patel, H.M. Simultaneous Determination of Brimonidine Tartrate and Timolol Maleate in Combined Pharmaceutical Dosage form Using Two Different Green Spectrophotometric Methods. *World J. Pharm. Pharm. Sci.* **2014**, *3*, 1330-1340.

(23) Toxicology Data Network, U.S. National Library of Medicine, https://toxnet.nlm.nih.gov/index.html, accessed in September 2018.

(24) Farha, O.K.; Eryazici, I.; Jeong, N.C.; Hauser, B.G.; Wilmer, C.E.; Sarjeant, A.A.; Snurr, R.Q.; Nguyen, S.T.; Yazaydin, A.Ö.; Hupp, J.T. Metal-Organic Framework Materials with Ultrahigh Surface Areas: Is the Sky the Limit?. *J. Am. Chem. Soc.* **2012**, *134*, 15016-15021.

(25) McKinstry, C.; Cussen, E.J.; Fletcher, A.J.; Patwardhan, S.V.; Sefcik, J. Scalable Continuous Production of High Quality HKUST-1 via Conventional and Microwave Heating. *Chem. Eng. J.* **2017**, *326*, 570-577.

(26) Tian, T.; Zeng, Z.; Vulpe, D.; Casco, M.E.; Divitini, G.; Midley, P.A.; Silvestre-Albero, J. Tan, J.-C.; Moghadam, P.Z.; Fairen-Jimenez, D. A Sol-gel Monolithic Metal-Organic Framework with Enhanced Methane Uptake. *Nature Mater.* **2018**, *17*, 174-179.

(27) Wang, S.; Yang, Q.; Zhong, C. Adsorption and Separation of Binary Mixtures in a Metal-Organic Framework Cu-BTC: A Computational Study. *Sep. Purif. Technol.* **2008**, *60*, 30-35.

(28) Getzschmann, J.; Senkovska, I.; Wallacher, D.; Tovar, M.; Fairén-Jimenez, D.; Düren, T.; van Baten, J.M.; Krishna, R.; Kaskel, S. Methane Storage Mechanism in the Metal-Organic Framework $Cu_3(btc)_2$: An in Situ Neutron Diffraction Study. *Microp. Mesop. Mater.* **2010**, *136*, 50-58.

(29) Lin, R; Ge, L.; Diao, H.; Rudolph, V.; Zhu, Z. Ionic Liquid as the MOFs/Polymer Interfacial Binder for Efficient Membrane Separation. *ACS Appl. Mater. Interfaces* **2016**, *8*, 32041-32049.

(30) Tan, F.; Liu, M.; Li, K.; Wang, Y.; Wang, J.; Guo, X.; Zhang, G.; Song, C. Facile Synthesis of Size-Controlled MIL-100(Fe) with Excellent Adsorption Capacity for Methylene Blue. *Chem. Eng. J.* **2015**, *281*, 360-367.

(31) Leclerc, H.; Vimont, A.; Lavalley, J.-C.; Daturi, M.; Wiersum, A.D.; Llewellyn, P.L.; Horcajada, P.; Ferey, G.; Serre, C. Infrared Study of the Influence of Reducible Iron(III) Metal

Sites on the Adsorption of CO, CO_2, Propane, Propene and Propyne in the Mesoporous Metal-Organic Framework MIL-100. *Phys. Chem. Chem. Phys.* **2011**, *13*, 11748.

(32) Valenzano, L.; Civalleri, B.; Chavan, S.; Bordiga, S.; Nilsen, M.H.; Jakobsen, S.; Lillerud, K.P.; Lamberti, C. Disclosing the Complex Structure of UiO-66 Metal Organic Framework: A Synergic Combination of Experiment and Theory. *Chem. Mater.* **2011**, *23*, 1700-1718.

(33) Karra, J.R.; Jasuja, H.; Huang, Y.-G.; Walton, K.S. Structural Stability of BTTB-based Metal-Organic Frameworks Under Humid Conditions. *J. Mater. Chem. A* **2015**, *3*, 1624-1631.

(34) ul Qadir, N.; Said, S.A.M.; Bahaidarah, H.M. Structural Stability of Metal Organic Frameworks in Aqueous Media - Controlling Factors and Methods to Improve Hydrostability and Hydrothermal Cyclic Stability. *Microp. Mesop. Mater.* **2015**, *201*, 61-90.

(35) Al-Janabi, N.; Hill, P.; Torrente-Murciano, L.; Garforth, A.; Gorgojo, P.; Siperstein, F.; Fan, X. Mapping the Cu-BTC Metal-Organic Framework (HKUST-1) Stability Envelope in the Presence of Water Vapour for CO2 Adsorption From Flue Gases. *Chem. Eng. J.* **2015**, *281*, 669-677.

(36) Gul-E-Noor, F.; Jee, B.; Pöppl, A.; Hartmann, M.; Himsl, D.; Bertmer, M. Effects of Varying Water Adsorption on a $Cu_3(BTC)_2$ Metal-Organic Framework (MOF) as Studied by ^{1}H and ^{13}C Solid-State NMR Spectroscopy. *Phys. Chem. Chem. Phys.* **2011**, *13*, 7783-7788.

(37) Orellana-Tavra, C.; Baxter, E.F.; Tian, T.; Bennett, T.D.; Slater, N.K.H.; Cheetham, A.K.; Fairen-Jimenez, D. Amorphous Metal-Organic Frameworks for Drug Delivery. *Chem. Commun.* **2015**, *51*, 13878-13881.

(38) Bakand. S. Cell Culture Techniques Essential for Toxicity Testing of Inhaled Materials and Nanomaterials In Vitro. *J. Tissue Sci. Eng.* **2016**, *7*, 1000181.

(39) Bernstein, S.L.; Kutty, G.; Wiggert, B.; Albert, D.M.; Nickerson, J.M. Expression of Retina-Specific Genes by Mouse Retinoblastoma Cells. *Invest. Ophtalmol. Vis. Sci.* **1994**, *35*, 3931-3937.

(40) Tan, E.; Ding, X.Q.; Saadi, A.; Agarwal, N.; Naash, M.I.; Al-Ubaidi, M.R. Expression of Cone-Photoreceptor-Specific Antigens in a Cell Line Derived From Retinal Tumors in Transgenic Mice. *Invest. Ophtalmol. Vis. Sci.* **2004**, *45*, 764-768.

(41) Chen, W.J.; Wu, C.; Kuse, Y.; Hara, H.; Duh, E.J. Nrf2 Protects Photoreceptor Cells From Photo-Oxidative Stress Induced by Blue Light. *Exp. Eye Res.* **2017**, *154*, 151-158.

(42) Fan, B.; Li, F.Q.; Zuo, L.; Li, G.Y. mTOR Inhibition Attenuates Glucose Deprivation-Induced Death in Photoreceptors via Suppressing a Mitochondria-Dependent Apoptotic Pathway. *Neurochem. Int.* **2016**, *99*, 178-186.

(43) Wyse Jackson, A.C.; Cotter, T.G. The Synthetic Progesterone Norgestrel is Neuroprotective in Stressed Photoreceptor-like Cells and Retinal Explants, Mediating its Effects via Basic Fibroblast Growth Factor, Protein Kinase A and Glycogen Synthase Kinase 3 β Signalling. *Eur. J. Neurosci.* **2016**, *43*, 899-911.

(44) Nixon, E.; Simpkins, J.W. Neuroprotective Effects of Nonfeminizing Estrogens in Retinal Photoreceptor Neurons. *Invest. Ophtalmol. Vis. Sci.* **2012**, *53*, 4739-4747.

(45) Januschowski, K.; Irigoyen, C.; Pastor, J.C.; Srivastava, G.K.; Romano, M.R.; Heimann, H.; Stalmans, P.; Van Keer, K.; Boden, K.; Szurman, P.; Spitzer, M.S. Retinal Toxicity of

Medical Devices Used during Vitreoretinal Surgery: A Critical Overview. *Ophthalmologica* **2018**, *240*, 236-243.